Electronic Research Archive

ERA, 33(4): 2391–2411.
DOI: 10.3934/era.2025106
Received: 06 March 2025
Revised: 11 April 2025
Accepted: 17 April 2025
Published: 22 April 2025

http://www.aimspress.com/journal/ERA

Research article

Modulation of epileptiform discharges by heterogeneous interneurons and external stimulation strategies in the thalamocortical model

Xiaojing Zhu, Yufan Liu, Suyuan Huang, Ranran Li and Yuan Chai*

School of Mathematics and Physics, Shanghai University of Electric Power, Shanghai 201306, China

* **Correspondence:** Email: chaiyuan@shiep.edu.cn.

Abstract: It is well known that inhibitory interneurons in the cerebral cortex can be classified as parvalbumin (PV), somatostatin subtypes (SOM), and vasoactive intestinal polypeptide subtypes (VIP) based on chemical characteristics. However, in models based on a corticothalamic model containing heterogeneous interneurons, the mechanisms underlying the dynamics of internal neurons and external stimuli are not well understood, and there are some challenges in selecting appropriate stimulation strategies. In this study, we first investigated and confirmed that insufficient feed-forward inhibition associated with PV neurons triggered seizures; second, we applied an optogenetic control strategy to confirm the control effect of excitatory optogenetic stimulation which targets either the PV or the SOM subtypes. Finally, we used a control strategy by applying both optogenetics and an electromagnetic induction stimulation to study the multiple possibilities of the dynamic evolution of seizures. The results confirmed that electromagnetic induction exhibits context-dependent effects in epileptic seizures, similar to the dual-effect phenomenon observed in previous studies, though with distinct network-level mechanisms in our thalamocortical model. In addition, a comparative analysis of the stimulation effects was performed. This work introduces a control scheme by combining internal neuronal pathways and external stimulation, thus providing new theoretical foundations and insights for the future treatment of epileptic seizures.

Keywords: absence seizures; optogenetic control; electromagnetic induction; hopf bifurcation; combined control strategy

1. Introduction

Absence epilepsy is a form of generalized epilepsy that is typically considered to be caused by abnormal interactions between the cortex and the thalamus [1]. In electroencephalogram (EEG) recordings, typical absence seizures are identified by the presence of either spike or polyspike wave discharges (p-SWDs) within the frequency range of 2.5–4 Hz [2,3], whereas atypical absence seizures exhibit a lower frequency, typically ranging from 1–2.5 Hz [4]. A prolonged polyspike ictal onset preceding generalized spike-and-waves at 3 Hz, which are associated with absence seizures, may indicate a poor response to treatment [5].

Neuronal electrophysiological activity is a complex process influenced by many factors. In fact, it has been observed in experiments that fluctuations in neuronal membrane potentials can generate time-varying magnetic fields [6]. Hence, it is necessary to consider electromagnetic induction in the nervous system [7]. Several studies have demonstrated that time-varying electromagnetic effects can be described by magnetic flux [8−10]. Moreover, a memristor has been employed to realize the coupling relationship between magnetic flux and membrane potential [11−13]. Through a bifurcation analysis, Duan et al. investigated the effects of direct and periodic currents on the membrane potential of individual neurons in the presence of magnetic flux effects [14]. Furthermore, the modulation of electromagnetic induction within the neuron-astrocyte coupling system was duly considered. The findings indicated that electromagnetic effects solely play a contributory role in the manifestation of temporal delays [15]. However, little is known about electromagnetic induction stimulation based on thalamocortical models containing cortical heterogeneous interneurons.

Recently, many scientists have begun using optogenetics to explore the working mechanisms of brain, including normal and abnormal network excitability. Optogenetics allows neurons to express light-sensitive ion channels through genetic modification and optical tools, thus enabling the activation or inhibition of specific neurons [16]. Emerging optogenetic techniques can selectively activate or inhibit certain neurons in complex brain regions with a minimal impact on other neurons [17]. In theoretical research, Nikolic et al. [18] successively established three-state and four-state mathematical models. Additionally, with the assistance of mesoscale models such as the Liley mean-field model, scholars have designed various open-loop and closed-loop optogenetic control strategies, thus leading to insights into the effectiveness of optogenetics in epilepsy control [19,20]. Although, optogenetic stimulations have made great progress in controlling epileptic seizures in the past few years, there has been little discussion regarding the combination of optogenetic stimulations and electromagnetic induction stimulations, which deserves further investigation.

To overcome these limitations, for the first time, we investigated the effects of feedforward inhibition strength associated with parvalbumin (PV) interneurons (specific relay nucleus (SRN) → PV → principal neuron (PN) pathway and somatostatin subtypes (SOM) → PV → PN pathway) and external controls including light and memristor stimulations on epileptic seizures in an extended thalamic cortex model. Furthermore, potential optogenetic stimulation targets for the treatment of epilepsy were explored, and a dual-target comprehensive regulation strategy of constructing electromagnetic induction stimulation targets and light stimulation targets was emphasized to reduce energy consumption [21]. The main contributions of this study are threefold. First, in a thalamic cortex model containing inhibitory neurons (PV, SOM, vasoactive intestinal polypeptide (VIP)), by adjusting the excitatory coupling from SRN to PV and the inhibitory coupling from PV to PN, the occurrence of pathological states can be internally controlled without adding external stimuli. Second, by separately

targeting inhibitory neurons PV and SOM and applying light stimulation, we can more easily reduce the occurrence of pathological states. Finally, using a control scheme of combining electromagnetic induction with light stimulation targeting PV and SOM neurons, we found that the addition of electromagnetic induction has a positive effect on the former and a reverse effect on the latter, further confirming that electromagnetic induction is a double-edged sword. Unlike previous studies that primarily focused on single-neuron electromagnetic models [11,13], our investigation employs a biologically realistic thalamocortical network which incorporates six distinct neural populations with experimentally validated connectivity. While the current clinical applications generally utilize single-modality approaches, our investigation of combined optogenetic and electromagnetic stimulations seeks to explore the potential synergistic effects that could enhance the therapeutic efficacy while reducing the energy requirements and side effects [20]. We hope this study can provide a new perspective for the clinical treatment of epileptic absences.

The organization of this paper is delineated as follows. Section 2 presents a description of the thalamocortical model and stimulus categories containing cortical heterogeneous interneurons. Section 3 first analyzes the main role of insufficient feedforward inhibition related to PV interneurons in triggering epileptic seizures, then explores the control effects of only adding light stimulation on epileptic seizures, thus adding light and memristor stimulations on the effects of epileptic seizures at the same time. Ultimately, electromagnetic induction proved to be a double-edged sword. In Section 4, we summarize the obtained results and discuss their limitations.

2. Model and stimulus description

2.1. Description of model

The thalamocortical model mainly consists of a thalamic module and a cortical module. In this study, we improved the neural field model proposed by Taylor et al. [22]. In addition, the model was extended to an augmented model containing cortical heterogeneous interneurons [23] to simulate more realistic cortical discharge dynamics and transitions between different oscillatory states. The thalamocortical model containing cortical heterogeneous interneurons is shown in Figure 1, where the cortical subsystem consists of PNs and three different types of inhibitory cells (PVs, SOMs, and VIPs), whereas the SRNs and the thalamic reticular nucleus (TRN) represent the thalamic subsystem. The gray arrow represents electromagnetic induction stimulation targeting PNs, while yellow dashed arrows indicate optogenetic stimulation targeting either PV neurons or SOM neurons. Lines with arrows and rounded heads indicate excitatory and inhibitory connections, respectively.

Mathematically, it can be described by the following differential equation [23]:

$$\frac{dPN}{dt} = \left(\dot{o}_{pn} - PN + p_1 f\left[PN\right] - p_2 f\left[PV\right] - p_3 f\left[SOM\right] + p_4 f\left[SRN\right] - E\right)\tau_{pn}, \tag{1}$$

$$\frac{dPV}{dt} = \left(\dot{o}_{pV} - PV + p_5 f\left[PN\right] - p_6 f\left[SOM\right] + p_{15} f\left[SRN\right] - p_{pp} f\left[PV\right] - U_{ChR2}^{pv}\right)\tau_{pv}, \tag{2}$$

$$\frac{dSOM}{dt} = \left(\dot{o}_{som} - SOM + p_7 f\left[PN\right] - p_8 f\left[PV\right] + p_{14} f\left[SRN\right] - p_{vip} f\left[VIP\right]\right)\tau_{som}, \tag{3}$$

$$\frac{dVIP}{dt} = \left(\dot{o}_{vip} - VIP + p_{pn} f\left[PN\right] - p_{pv} f\left[PV\right] - p_{som} f\left[SOM\right] + p_{srn} f\left[SRN\right]\right)\tau_{vip}, \tag{4}$$

$$\frac{dSRN}{dt} = \left(\dot{o}_{srn} - SRN + p_{10} f\left[PN\right] - p_9 z\left[TRN\right]\right)\tau_{srn}, \tag{5}$$

$$\frac{dTRN}{dt} = \left(\dot{o}_{trn} - TRN + p_{13} f\left[PN\right] + p_{12} z\left[SRN\right] - p_{11} z\left[TRN\right]\right)\tau_{trn}, \tag{6}$$

where *PN*, *PV*, *SOM*, *VIP*, *SRN*, and *TRN* correspond to the average membrane potentials of each neural population. Meanwhile, ϵ_i and τ_i stand for the additive constant and time parameters, respectively. i = *pn, pv, som, vip, srn, trn.* p_1, p_2, p_3, ..., p_{15}, p_{pn}, p_{pp}, p_{pv}, p_{som}, p_{vip}, p_{srn} signifies the synaptic connectivity strength between the neuronal populations. U_{ChR2}^{pv} is employed for light stimulation control, and its detailed description can be found in 2.3.

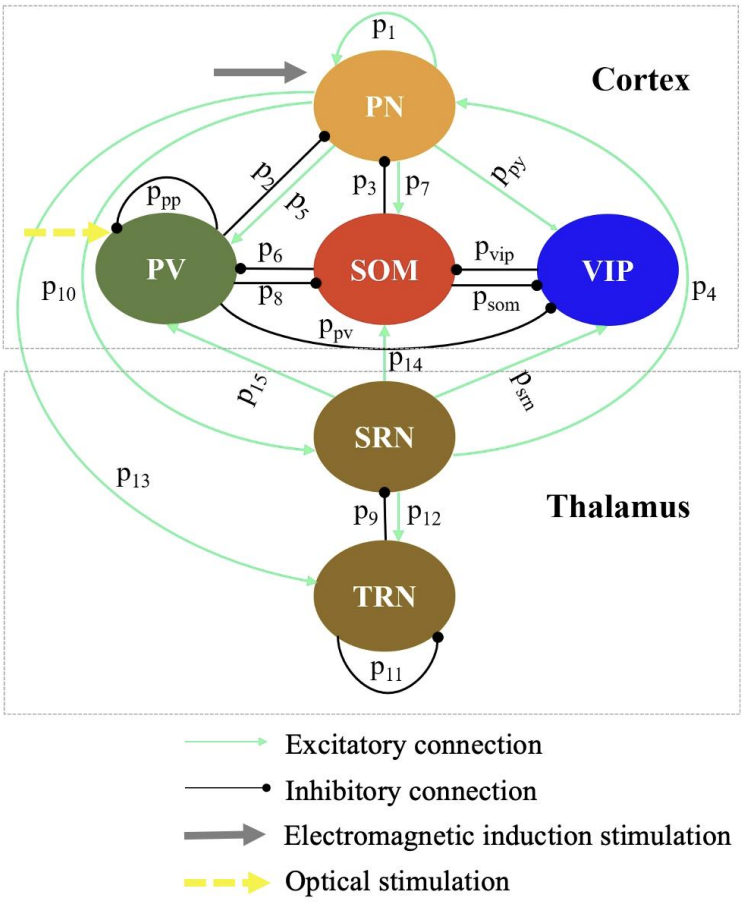

Figure 1. Schematic diagram of the thalamocortical model featuring cortical interneurons with diverse characteristics. Within the cortical subsystem, there exists an excitatory population (PN) alongside three distinct inhibitory populations (PV, SOM, and VIP). The SRN and TRN are indicative of the thalamic subsystem.

Table 1. Constant parameter values used in the thalamocortical model.

Parameters	Interpretation	Value	Parameters	Interpretation	Value
p_1	PN→PN	1.8	p_{vip}	VIP→SOM	1
p_2	PV→PN	Varied	p_{srn}	SRN→VIP	1
p_3	SOM→PN	1.38(1.45)	p_{pp}	PV→PV	2
p_4	SRN→PN	1	$\grave{o}_{pn}$	Input PN	–0.35
p_5	PN→PV	4.5	$\grave{o}_{pv}$	Input PV	–3.5
p_6	SOM→PV	0.5(2)	$\grave{o}_{som}$	Input SOM	–3.4
p_7	PN→SOM	4	$\grave{o}_{vip}$	Input VIP	3.3
p_8	PV→SOM	0.2	$\grave{o}_{srn}$	Input SRN	–2
p_9	TRN→SRN	0.5	$\grave{o}_{trn}$	Input TRN	–5
p_{10}	PN→SRN	3.5	τ_{pn}	PN timescale	0.026 ms^{-1}
p_{11}	TRN→TRN	0.2	τ_{pv}	PV timescale	0.065 ms^{-1}
p_{12}	SRN→TRN	10.5	τ_{som}	SOM timescale	0.0325 ms^{-1}
p_{13}	PN→TRN	3	τ_{vip}	VIP timescale	0.0325 ms^{-1}
p_{14}	SRN→SOM	0.2	τ_{srn}	SRN timescale	0.0026 ms^{-1}
p_{15}	SRN→PV	Varied	τ_{trn}	TRN timescale	0.0026 ms^{-1}
p_{pn}	PN→VIP	3.5	ν	Sigmoid steepness	2.5×10^5
p_{pv}	PV→VIP	0.5	α	Constant	2.8
p_{som}	SOM→VIP	1	β	constant	0.5

Moreover, $f[.]$ and $z[.]$ are activation functions with the following forms:

$$f(x) = \left(1/\left(1+v^{-x}\right)\right), \tag{7}$$

$$z(y) = \alpha y + \beta, \tag{8}$$

where x = *PN*, *PV*, *SOM*, *VIP*, *SRN*, *TRN*. y = *SRN*, *TRN*. The steepness of the two activation functions is dictated by v and α, with β held constant at 0.5. The parameters in the model are consistent with previous studies, and the values of the constant parameters are listed in Table 1. The thalamocortical model parameters are consistent with previous studies [22,23], which have been calibrated to replicate the key electrophysiological features of absence epilepsy.

2.2. Electromagnetic stimulation

Neuronal electrophysiological activity is a complex process influenced by various factors. In fact, it has been experimentally observed that time-varying magnetic fields can be induced, which is attributed to fluctuations in the neuronal membrane potential [11,13]. As shown in Figure 1, the cortical subsystem includes the excitatory pyramidal neuronal population (PN) and the inhibitory cells (PV, SOM, and VIP). Here, we only consider the electromagnetic induction of the pyramidal neuron population induced by the dominant action of pyramidal neurons. The stimulation of the memristor E is defined as follows:

$$E = g_0 * \rho(\phi) * PN, \tag{9}$$

$$\frac{d\phi}{dt} = g_1 * PN - g_2 * \phi, \tag{10}$$

$$\rho(\phi) = m_1 + 3n_1 * \phi^2. \tag{11}$$

The variable ϕ represents the average magnetic flux across the membrane, and $\rho(\phi)$ is the memristor's memory conductance. m_1 and n_1 are fixed parameters. g_0, g_1, and g_2 are parameters associated with electromagnetic induction. g_1 and g_2 reflect the influence of pyramidal neurons on the average magnetic flux, while g_0 represents the feedback gain of the average magnetic flux.

The electromagnetic induction parameters listed in Table 2, including flux feedback gain and self-inductance effect, are derived from the memristor-based framework established by Wu and Ma [13], which has been validated through experimental measurements of neuronal magnetic fields. You can find the corresponding parameter values from Table 2.

Table 2. Parameters related to electromagnetic induction stimulation.

Parameters	Interpretation	Value
g_0	Flux feedback gain	2.6
g_1	Gain from PY	–6
g_2	Self-inductance effect gain	130
m_1	Constant	0.4
n_1	Constant	0.02

2.3. Optogenetic stimulation

Scholars have demonstrated that optogenetic stimulation can effectively control seizures in the cerebral cortex [24,25]. The four-state model can qualitatively reproduce the ChR2 photocurrent, and the characteristic peak-platform behavior observed from experimental measurements [26]. Here, taking cues from the study conducted by [27], we employ a four-state model to simulate the dynamics of photocurrent as follows:

$$\frac{do_1}{dt} = H_{a1}l_1 - \left(K_{d1} + e_{12}\right)o_1 + e_{21}o_2, \tag{12}$$

$$\frac{do_2}{dt} = H_{a2}l_2 + e_{12}o_1 - \left(K_{d2} + e_{21}\right)o_2, \tag{13}$$

$$\frac{dl_1}{dt} = K_r l_2 + K_{d1} * o_1 - H_{a1} * l_1, \tag{14}$$

$$\frac{dp}{dt} = \frac{Q_0(\theta) - p}{\tau_{ChR2}}, \tag{15}$$

$$o_1 + o_2 + l_1 + l_2 = 1. \tag{16}$$

where o_1, o_2 (or l_1, l_2) represent the fraction of channels in various open (or closed) states. p is a state variable. H_{a1}, H_{a2}, e_{12}, e_{21}, K_{d1}, K_{d2}, and Kr are transition rates. $Q_0(\theta)$ is an activation function. τ_{ChR2} is the time constant. In addition, the form of the photocurrent is as follows:

$$I_{ChR2}^{x} = b_{ChR2} * W\left(S_x\right) * \left(o_1 + \gamma o_2\right)\left(S_x - E_{ChR2}\right). \tag{17}$$

Table 3. Parameters related to optogenetic stimulation.

Parameters	Interpretation	Value
H_{a1}	Transition rate $L_1 \rightarrow O_1$	$\eta_1 J * p(\text{ms}^{-1})$
H_{a2}	Transition rate $L_2 \rightarrow O_2$	$\eta_2 J * p(\text{ms}^{-1})$
K_{d1}	Transition rate $O_1 \rightarrow L_1$	$0.075 + 0.043 * \tanh(-(S_x + 20)/20)(\text{ms}^{-1})$
K_{d2}	Transition rate $O_2 \rightarrow L_2$	$0.05(\text{ms}^{-1})$
e_{12}	Transition rate $O_1 \rightarrow O_2$	$0.011 + 0.005\ln(1 + E_x/0.024)(\text{ms}^{-1})$
e_{21}	Transition rate $O_2 \rightarrow O_1$	$0.008 + 0.004\ln(1 + E_x/0.024)(\text{ms}^{-1})$
K_r	Transition rate $Z_2 \rightarrow Z_1$	$4.34587 * 10^{-5} * \exp(-0.0211539274 * S_x)(\text{ms}^{-1})$
η_1	Z1 Quantum efficiency of absorbed photons	0.8535
η_2	Z2 Quantum efficiency of absorbed photons	0.14
J	Photon flow	$\sigma_{ret} * E_x * \lambda / (w_{loss} * h * c)(\text{ms}^{-1})$
σ_{ret}	Retinal absorption cross section	$10^{-20}\ \text{m}^2$
$E_{\text{pv/som}}$	Light irradiance of target population	Varied(mW/ mm^2)
λ	Optical wavelength	470 nm
w_{loss}	Photon Loss Scaling Factor	1.3
h	Planck's constant	$6.626 * 10^{-34}$ Js
c	Light speed	$3 * 10^8$ m/ s
$Q_0(\theta)$	ChR2 activation function	$0.5 * (1 + \tanh(120(100E_x - 0.1)))$
τ_{ChR2}	The activation time constant of ChR2	1.3 ms
b_{ChR2}	Maximum conductance for ChR2	400 nS
γ	Conductivity ratio	0.1
E_{ChR2}	The reversal potential of ChR2	0 mV
$\varepsilon_{pv/som/vip}$	Slope of linear transformation	60 mV
$\mu_{pv/som/vip}$	The intercept of a linear transformation	20 mV
R_m	Average resistance of stimulated population	3.2 MΩ
N_{ChR2}	The number of ChR2 channels	$2.5 * 10^2$

The rectifying function related to voltage satisfies the following:

$$W(S_x) = \left[10.6408 - 14.6408 * exp\left(-\frac{S_x}{42.7671} \right) \right] / S_x \tag{18}$$

where S_x is the membrane potential. b_{ChR2} is the maximum conductance. $\gamma = b_2 / b_1$, where b_1, b_2 are the maximum conductance in states o_1 and o_2, respectively. Referring to previous studies [28,29], we linearly transform the membrane potential from the population level (PV, SOM, and VIP) to the neuron level S_x applied in Eqs (15) and (16). That is to say, $S_x = \varepsilon_x x - \mu_x$, $x = pv, som, vip$. The control potential induced by light stimulation is defined as follows:

$$U_{ChR2}^{x} = I_{ChR2}^{x} N_{ChR2} R_m / \varepsilon_x \tag{19}$$

where R_m is the average resistance of the stimulated population, and N_{ChR2} represents the density of ChR2 channels per unit area. The numerical values and specific meanings of the related parameters are shown in Table 3.

3. Numerical results and discussion

In the study, we used three different protocols to modulate SWD and induce transitions between different states. Initially, there is no stimulus added to simulate an absence seizure induced by abnormal SRN → PV → PN projections, which has been uncovered in many experiments and is used here to validate the model. Second, we adopt optogenetic stimulation targeting PV or SOM neurons to achieve seizure control. Finally, on this basis, we explored the effects of applying optogenetic stimulation targeting PV and SOM neurons along with the addition of electromagnetic induction stimulation on the control of seizures, more importantly, compared the effects of different stimulation regimens (addition of optogenetic stimulation only, simultaneous addition of optogenetic stimulation, and electromagnetic induction stimulation) on the control of seizures.

Numerical simulations are performed in the MATLAB environment using the fourth-order Runge-Kutta method. For the no-stimulus case, we set a fixed time step of 1 ms, thus allowing the time series to essentially reach stability. When adding the light stimulus, we consider the photodynamics and set the fixed time step to 0.01 ms [30−32]. The polar plots illustrate the maximum and minimum values. The extrema of the PN membrane potential were computed using MATLAB's 'findpeaks' function (prominence threshold = 0.1 mV, minimum peak distance = 50 ms). The steady-state intervals (last 2s of simulations) were analyzed to classify the dynamical states. A Fast Fourier Transform (FFT) is used to perform the analysis of the dominant frequency of the oscillatory state, while the dominant frequency corresponding to the dormant state is set to 0.

3.1. Effect of thalamic feedforward inhibition of PV interneurons on seizures

First, we present the different firing state patterns observed in our thalamocortical model containing heterogeneous interneurons. Figure 2 illustrates a time series corresponding to several distinct dynamical states that can emerge depending on the system parameters. The different firing patterns shown in Figure 2 arise from changes in the network connectivity, particularly the strength of

the feedforward inhibition associated with PV interneurons. To understand the mechanisms underlying these transitions, we now analyze how these states evolve with changing parameter values through a bifurcation analysis.

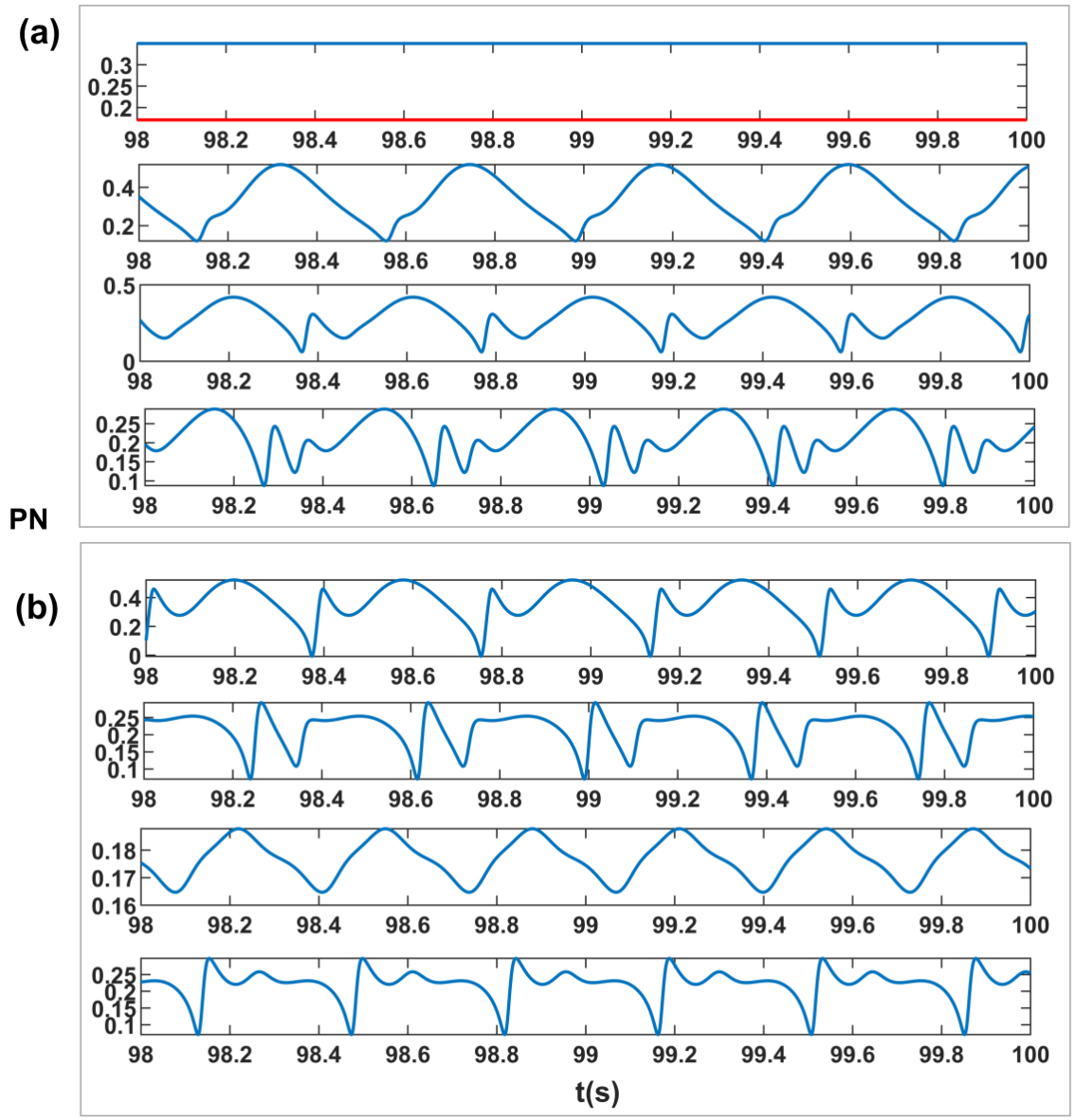

Figure 2. Time series corresponding to different states. (a) Low saturated state, $p_{15} = 2$, $p_2 = 0.5$ (red line), high saturated state, $p_{15} = 2$, $p_2 = 0.05$. Clonic state, $p_{15} = 0.55$, $p_2 = 0.12$. SWDs, $p_{15} = 1$, $p_2 = 0.3$. 2-SWDs, $p_{15} = 1$, $p_2 = 0.5$. (b) SWDs, $p_{15} = 1$, $p_2 = 4$. 2-SWDs, $p_{15} = 4$, $p_2 = 0.4$. Simple oscillation, $p_{15} = 3.2$, $p_2 = 1.6$. Other wave, $p_{15} = 2.4$, $p_2 = 3$. Other parameter values are selected according to Table 1. Parameter values for (a): $p_3 = 1.38$, $p_6 = 0.5$; for (b): $p_3 = 1.45$, $p_6 = 2$. Other parameter values are selected according to Table 1.

First, we set two sets of initial values for the SOM → PV inhibition, high and low, respectively. Figure 3(a),(b) corresponds to the relatively weak and relatively strong inhibition of the PV by the

SOM. The terms 'weak' and 'strong' refer to the relative inhibition levels mediated by SOM → PV coupling. It can be found that the inhibition of SOM → PN may dominate when the SOM → PV coupling is relatively less. From Figure 3(a) single-parameter polar plots, as p_{15} increases, the system changes from an initial high saturation state to a typical SWD state of an apoplectic seizure, which consists of two maxima and minima, then to a state in which SWDs and low saturation coexist. As p_{15} further increases, it can convert the system from a pathological state to a normal state. Figure 4 shows the corresponding bifurcation diagram. Hopf bifurcations (HB_1) mark transitions to oscillatory states (e.g., SWD), while Limit Point of Cycles (LPC) bifurcations indicate seizure suppression. These thresholds are modulated by p_{15} and p_2. Figure 4(a) shows the corresponding bifurcation diagram, and it can be found that with a further increase of p_{15}, the appearance of a Hopf bifurcation leads to the coexistence of the low saturation state with SWD. The pathological waveform completely disappears after the LPC_1 bifurcation (i.e., the seizure is completely controlled).

We conducted the same validation for the case with a relatively strong projection from SOM to PV interneurons. The corresponding bifurcation diagram is shown in Figure 4(b), where it can be observed that in terms of the bifurcation structure, there is no folding of the periodic bifurcation (LPC), while the oscillatory solution directly arises from the HB_1 bifurcation point, which implies that there is a simple oscillation rather than a clone state. As p_{15} increases, we observe that after the LPF_2 bifurcation point, the low saturation state persists, either coexisting with other states or alone, depending on the choice of the initial value, and the system is likely to be successfully inhibited.

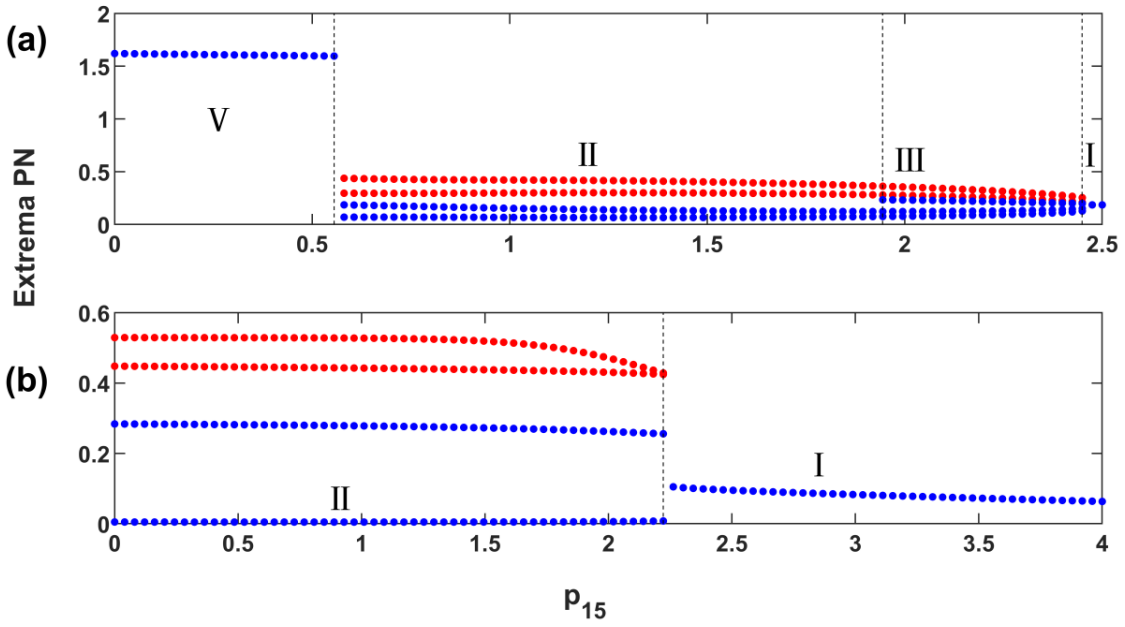

Figure 3. Extreme diagram showing the extrema mean of PN, where the red and blue colors represent the maximum and minimum values, respectively. (a) Changes in the extremes of PN as p_{15} increases. Take $p_2 = 0.3$, $p_3 = 1.38$, $p_6 = 0.5$; (b) Changes in the extremes of PN as p_{15} increases. Take $p_2 = 5$, $p_3 = 1.45$, $p_6 = 2$.

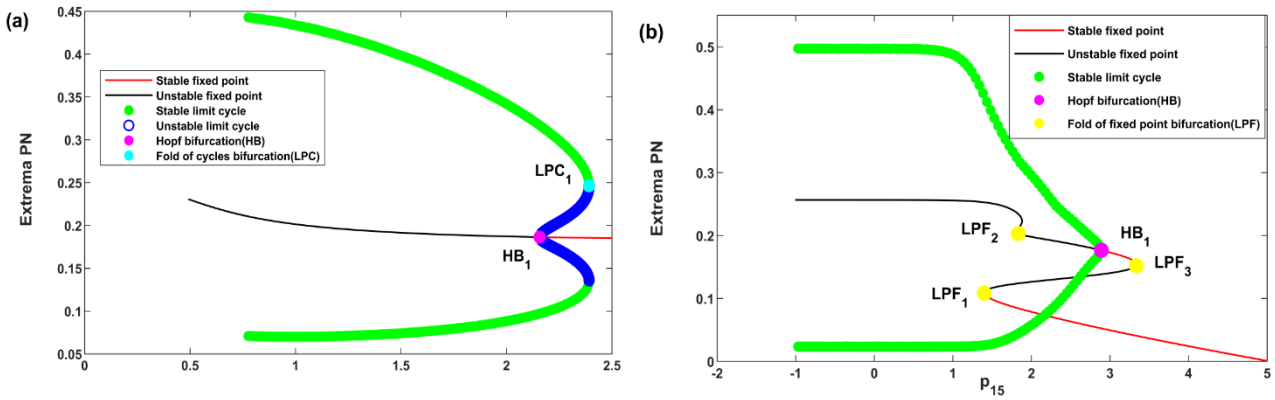

Figure 4. Bifurcation plots of the dynamics corresponding to Figure 3 for (a) when the suppression of PV by SOM is weak and (b) when the suppression of PV by SOM is strong. The pink marking points indicate a fold of Hopf bifurcations.

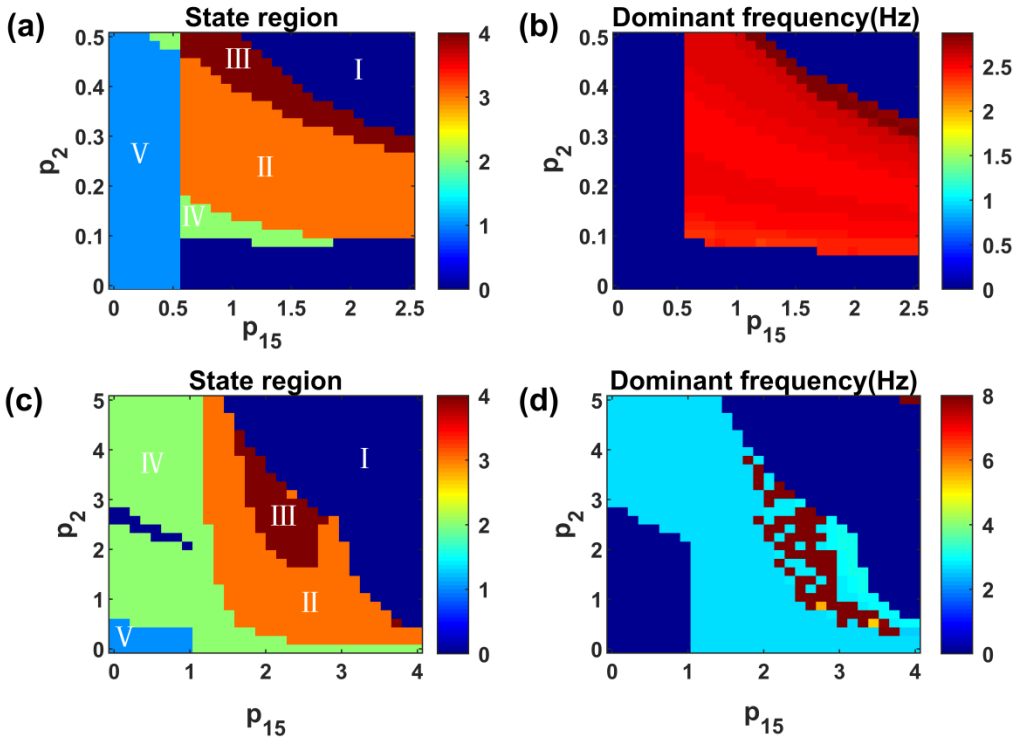

Figure 5. Dynamic analysis in the panel (p_{15}, p_2) and their dominant frequency. (a) Dynamical evolution of the PN under the combined effect of the SRN → PV connection strength (p_{15}) and the PV → PN connection strength (p_2). $p_3 = 1.38$, $p_6 = 0.5$. (b) Main frequency analysis which corresponds to (a). (c) Dynamical evolution of the PN under the combined effect of the SRN → PV connection strength (p_{15}) and the PV → PN connection strength (p_2). $p_3 = 1.45$, $p_6 = 2$. (d) Main frequency analysis which corresponds to (c).

Second, through Figure 5, we find that the thalamus produces a sufficiently strong feed-forward inhibition of PV interneurons to help maintain a normal activity, regardless of whether the SOM INS inhibits the PV INS relatively weakly or relatively strongly. Observations from Figure 5(a),(b) indicate

that robust connections from the SRN to PV interneurons, as well as from the PV interneurons to PNs, enable normal feedforward inhibition. This leads to the effective suppression of PNs to a low saturation health state (I). A reduced strength in either of these connections results in an increased excitability of PNs, thus leading to epileptiform discharges such as SWDs (II) and 2-SWDs (III). When the coupling strength is very weak, the system tends to converge towards either clonic activity (IV) or a state of heightened excitability with a higher saturation threshold (V).

Similar findings were observed when the SOM interneurons were configured to strongly inhibit the PV interneurons. This can lead to a dominance of disinhibition from the SOM interneurons. Figure 5(c),(d) show that an inadequate projection strength from the SRN to PV and from the PV to PY neurons still results in SWDs (II), 2-SWDs (III), and even a high saturation state. In comparison to Figure 5(a),(b), higher coupling strengths are needed to control seizures in this scenario.

3.2. Effect of of adding optogenetic stimulation on the control of epileptic seizures.

Scholars have revealed that PV interneurons emerge as a promising target for seizure treatment [33,34]. Therefore, we applied excitatory light stimulation to PV interneurons and SOM neurons, which can be seen in Figure 6(a). With the increase of light intensity, the PN shifted from a state of high saturation alongside 2-SWDs to the SWD state and was successfully suppressed to the low-saturation healthy state (I). A similar effect can be seen from Figure 6(b), where the PN is successfully suppressed from the SWD state to the low-saturation healthy state, with a portion of other states in between, which is not the focus of our study. In fact, the efficacy of inhibition is not solely determined by the strength of connections with the PN population, but also hinges on the intrinsic firing patterns of the neuronal ensemble. Both thalamic projections and light stimulations are directed towards augmenting the excitability of the PV population, which could explain the similarity between these two regulatory mechanisms. On the other hand, light stimulation was performed on the SOM INS rather than the PV INS. There is evidence that excitation of the SOM also plays a role in controlling seizures [35,36]. As can be seen in Figure 6(b), increasing the light intensity eliminates the 2-SWDs and ultimately suppresses the PNs to a low saturated state with other oscillatory intervals (not specifically discussed). This demonstrates the important role of the SOM $\rightarrow$ PN projection in the circuit.

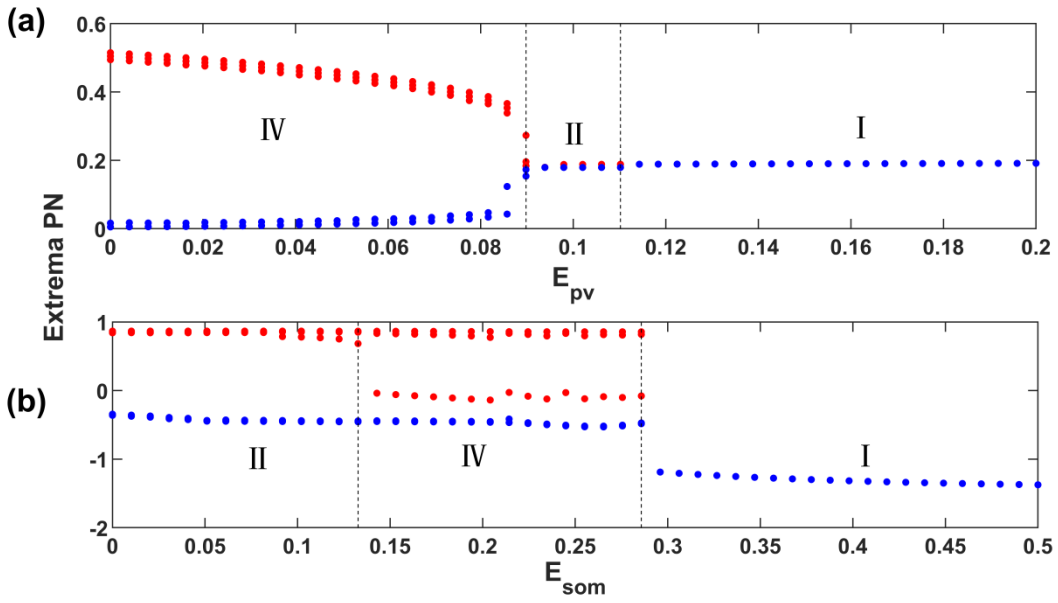

Figure 6. The extreme diagram showing the extrema mean of PN, where the red and blue colors represent the maximum and minimum values, respectively. Take $p_2 = 0.2$, $p_3 = 1.45$, $p_6 = 2$, $p_{15} = 1.5$; (a) Changes in the extremes of PN as E_{pv} increases. (b) Changes in the extremes of PN as E_{som} increases.

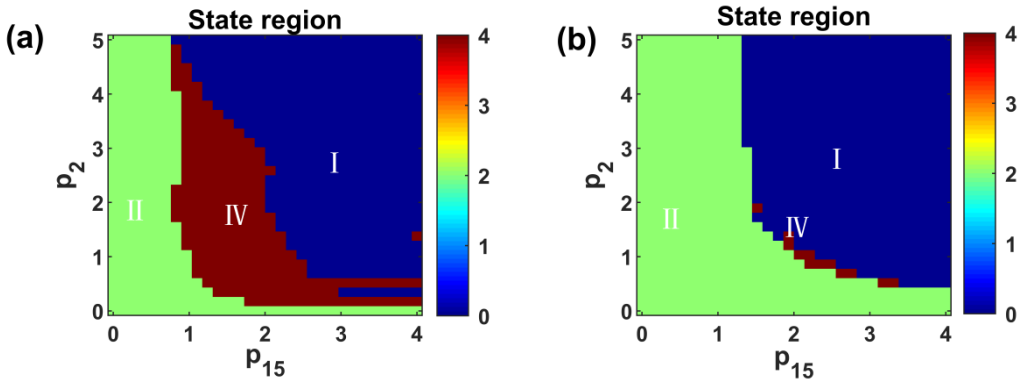

Figure 7. Dynamic analysis in the panel (p_{15}, p_2) of applied light stimulation. Take $p_3 = 1.45$, $p_6 = 2$. (a) Targeting PV neurons with light stimulation, $E_{pv} = 0.01$. (b) Targeting SOM neurons with light stimulation, $E_{som} = 0.06$. Blue regions indicate low-saturation (healthy) states, while other colors represent various pathological states.

To explore the effect of a sufficiently strong light stimulation on the control of epileptic seizures of different degrees, we targeted the PV and SOM neurons and applied a continuous light stimulation with an intensity of 0.01 to each point on the two-parameter plane of Figure 5(c), as shown in Figure 7(a),(b).

After applying light stimulation to the targeted PV neurons and comparing to Figure 5(c), we can find that the area of the pathological state is greatly reduced, and the light stimulation plays a good role in controlling epilepsy. However, we found that the stimulation did not eliminate the pathological waveforms caused by smaller coupled connections because the states were overexcited, which could

also be interpreted as a deeper pathology; therefore, a stronger light was needed for control purposes.

3.3. Effect of adding optogenetic stimulation and electromagnetic induction stimulation on controlling epileptic seizures.

In the previous subsection, we separately targeted PV and SOM for optical stimulations and demonstrated an effective therapeutic effect through a reduction in the status epilepticus. However, it is not clear how effective the control of seizures will be when it is applied in combination with other stimulation protocols, such as an electromagnetic induction. In this section, we focus on the effects of the simultaneous addition of optical stimulation and electromagnetic induction on seizures and discuss the changes in the status quo when the intensity of the optical stimulation and electromagnetic induction are varied.

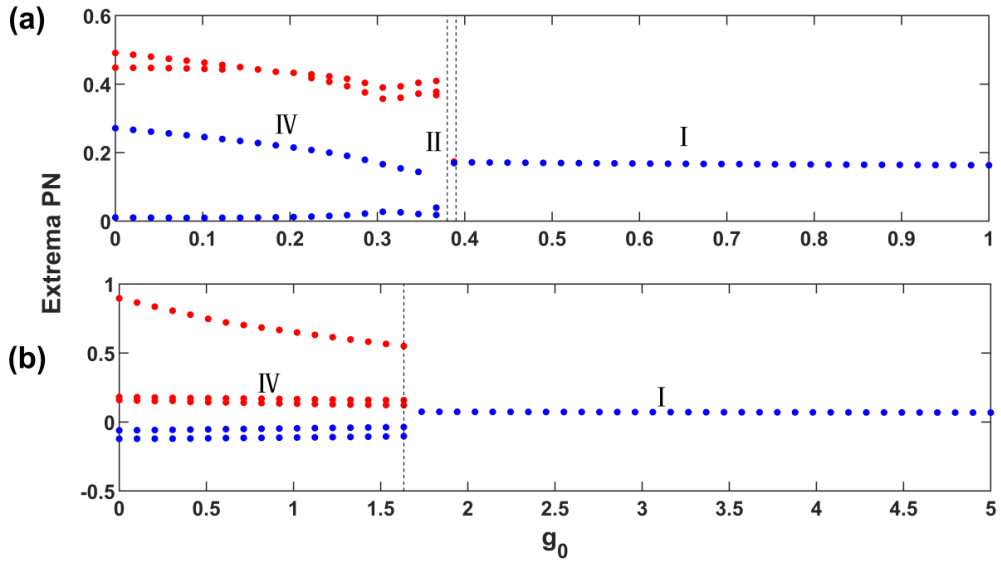

Figure 8. Extreme diagram showing the extrema mean of PN, where the red and blue colors represent the maximum and minimum values, respectively. Take $p_2 = 0.15$, $p_3 = 1.45$, $p_6 = 2$, $p_{15} = 0.9$. (a) Changes in the extremes of PN as g_0 increases with PV-targeted optical stimulation, $E_{pv} = 0.06$. (b) Changes in the extremes of PN as g_0 increases with SOM-targeted optical stimulation, $E_{som} = 0.06$.

When targeting the PV neurons with both optical stimulation and electromagnetic induction stimulation, from Figure 8(a), it can be seen that the system shifted from a 2-SWD state to a transient clonic state when the feedback gain from magnetic flux increased and was eventually successfully suppressed to a low-saturation state as the amnesia strength continued to increase. Similarly, when both optical stimulation and electromagnetic induction stimulation were applied to the targeted SOM neurons, from Figure 8(b), it can be seen that the system gradually shifted from a pathological state to a healthy low-saturation state as g_0 increased. However, since the state transition is sensitive to the initial value, we also plotted the state dynamics of the two-parameter change to verify the accuracy of the above conclusion by the change of the two-parameter.

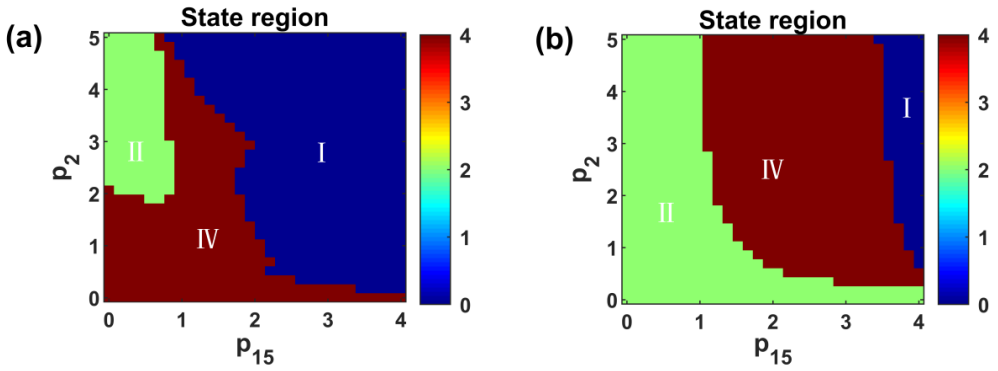

Figure 9. Dynamic analysis in the panel (p_{15}, p_2) of applied light stimulation and electromagnetic induction. Take $p_3 = 1.45$, $p_6 = 2$, $g_0 = 0.1$. (a) Targeting PV neurons with light stimulation, $E_{pv} = 0.06$. (b) Targeting SOM neurons with light stimulation, $E_{som} = 0.06$.

Figure 9(a),(b) show the dynamic panel of the two-parameter state with both light stimulation and electromagnetic induction added. Comparing Figures 7(a) and 9(a), it can be clearly seen that the normal low saturation state area is more in Figure 9(a), which means that the imposition of electromagnetic induction stimulation has a good effect on seizures. However, when electromagnetic induction stimulation and light stimulation were simultaneously applied to the target SOM, a comparison of Figures 7(b) and 9(b) shows that the area of the blue region in the state diagram of Figure 9(b) decreased, which implies that the area of the pathological state was larger, and that the over-suppression of the SOM required stronger light to a certain extent, suggesting that electromagnetic induction is a double-edged sword.

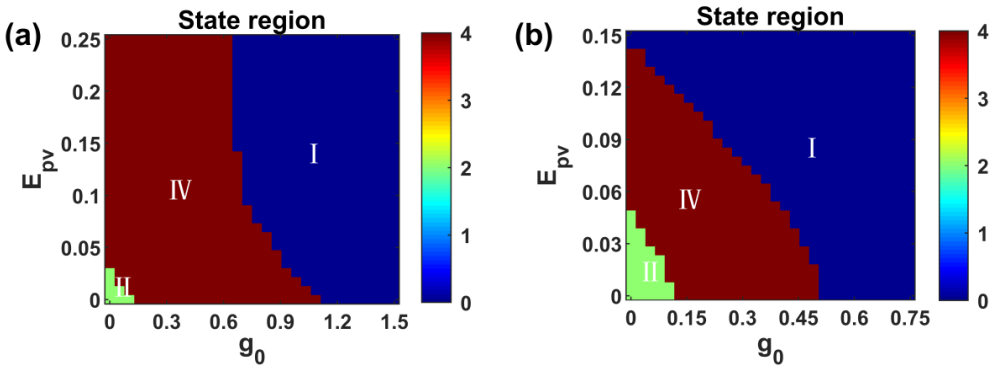

Figure 10. Dynamic analysis in the panel of the feedback gain from magnetic flux and excitatory light irradiance on PV. The color regions represent different dynamical states, with blue indicating healthy states and other colors showing various pathological states. (a). Take p_3=1.38, p_6 =0.5. (b). Take $p_3 = 1.45$, $p_6 = 2$; Other parameter values are selected according to Table 1.

To further investigate the effects of electromagnetic induction stimulation and optical stimulation on the dynamic shift of the system, we set the coupling of the SOM → PV pathway in two groups as before. This enables a more comprehensive study of the feedforward inhibition associated with PV neurons in relation to external stimulation.

From the two-dimensional panel of light intensity versus electromagnetic induction intensity, it can be observed that the effects of the electromagnetic induction feedback and the intensity of optical stimulation applied against the PV neurons on the inhibition of epilepsy are in the same direction.

As shown in Figure 10(a), with a relatively weak inhibition of PV interneurons by SOM, sufficiently strong feed-forward inhibition produced by the thalamus acting on the PV interneurons helps to maintain normal activity. In contrast to Figure 10(b), it requires a greater intensity of light and electromagnetic induction feedback to transform the system into a healthy state. In addition, a smaller g_0 does not alter the state with increasing light irradiance compared to when there is no electromagnetic field ($g_0 = 0$). g_0 enhancement can cause the typical 2-SWD to disappear.

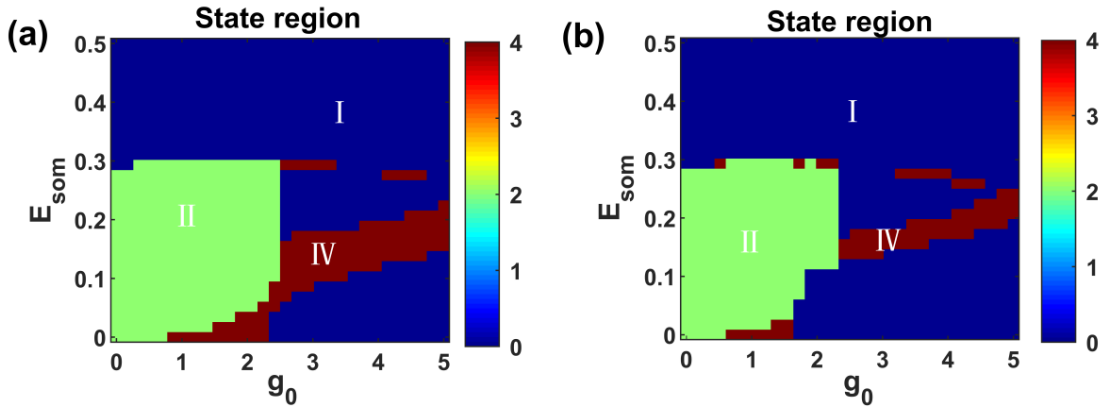

Figure 11. Dynamic analysis in the panel of the feedback gain from magnetic flux and excitatory light irradiance on SOM. The color regions represent different dynamical states, with blue indicating healthy states and other colors showing various pathological states. (a). Take p_3=1.38, p_6 =0.5. (b). Take p_3 = 1.45, p_6 = 2; Other parameter values are selected according to Table 1.

Figure 11 shows the co-modulation of the optical stimulus intensity and feedback gain g_0 applied to SOM neurons. However, unlike the co-stimulation applied to the PV neurons shown in Figure 10, the effects of light stimulation and electromagnetic induction stimulation targeting SOM neurons (Figure 11) do not have aligned effects on seizure control, but instead show a more complex relationship. Overall, increasing g_0 required a decreased light intensity to control the system to a healthy state, thus suggesting some control of seizures by electromagnetic induction.

3.4. Comparative analysis of stimulation strategies.

Our results uncover significant mechanistic and functional disparities between optogenetic and electromagnetic stimulation in seizure control. Optogenetics directly activates specific interneuron populations via ChR2. It strengthens feedforward inhibition to suppress hyperactive principal neurons, thus offering precise temporal and cell - type control. However, it demands a careful intensity calibration [24,25]. Conversely, electromagnetic induction modulates the PN activity through memristor - coupled magnetic flux (g_0), globally altering the bifurcation thresholds [11,13,37]. In our study, its “double - edged sword” effect, seen in single - neuron models [37], is extended to network - level dynamics. As shown in Figure 8, increasing g_0 can shift the system from pathological

to healthy low - saturation states, with the efficacy varying by the neural pathway.

These mechanistic distinctions lead to different efficacy profiles. The optogenetic stimulation rapidly suppresses frequencies but may need high energy inputs. Electromagnetic stimulation has more complex effects: it moderately reduces the pathological states, thereby stabilizing PV - targeted pathways while potentially destabilizing SOM - targeted ones. Combining PV - targeted optogenetics with electromagnetic stimulation brings synergistic advantages. It requires less energy and enhances the suppression efficacy. Previous reviews [38] have emphasized the potential of such combinatorial approaches in epilepsy therapy. Multimodal stimulation strategies may overcome single - technique limitations. Our findings highlight the promise of multimodal approaches in optimizing seizure management, as the combination of optogenetic targeted cellular control and electromagnetic induction - based network modulation could offer more effective and efficient therapeutic interventions than single - approach methods.

4. Conclusions

In conclusion, our study highlighted the importance of inhibitory mechanisms, particularly thalamic feedforward inhibition of PV interneurons, in controlling epileptic seizures. First, by adjusting internal couplings, we demonstrated the potential for an internal control of pathological states. Specifically, the modulation of excitatory and inhibitory connections within the thalamic cortex model, which contains inhibitory neurons such as PV, SOM, and VIP, revealed promising avenues for seizure regulation. Second, by targeting specific inhibitory neurons and applying light stimulation, we observed a significant reduction in the pathological states. This targeted approach offers a promising strategy for seizure management, thereby potentially enhancing the precision and effectiveness in intervention strategies for patients with epilepsy. Lastly, the synergistic effects of the innovative combination of optogenetic and electromagnetic induction stimulations revealed a dual impact on PV and SOM neurons. Our findings demonstrate effective seizure control in some neurons while exhibiting contrasting effects on others.

These findings reveal the importance of interdisciplinary research and personalized treatment strategies in advancing epilepsy management. However, our study is limited to research and computational evidence solely based on this model. Future studies could explore experiments based on different models and further validate these findings through physiological experiments to enhance the persuasiveness of our discoveries and achieve better seizure control outcomes.

Use of AI tools declaration

The authors declare they have not used Artificial Intelligence (AI) tools in the creation of this article.

Acknowledgments

This work was supported by the National Natural Science Foundation of China (Grant Nos. 12271342, 11502139).

Conflict of interest

The authors declare there is no conflict of interest.

References

1. O. C. Snead, Basic mechanisms of generalized absence seizures, *Ann. Neurol.*, **37** (1995), 146–157. https://doi.org/10.1002/ana.410370204
2. C. P. Panayiotopoulos, Typical absence seizures and related epileptic syndromes: assessment of current state and directions for future research, *Epilepsia*, **49** (2008), 2131–2139. https://doi.org/10.1111/j.1528-1167.2008.01777.x
3. F. Marten, S. Rodrigues, O. Benjamin, M. P. Richardson, J. R. Terry, Onset of polyspike complexes in a mean-field model of human electroencephalography and its application to absence epilepsy, *Philos. Trans. R. Soc. A: Math., Phys. Eng. Sci.*, **367** (2009), 1145–1161. https://doi.org/10.1098/rsta.2008.0255
4. P. Jain, Absence Seizures in Children: Usual and the Unusual, *Indian J. Pediatr.*, **87** (2020), 1047–1056. https://doi.org/10.1007/s12098-019-03135-8
5. W. O. Tatum, S. Ho, S. R. Benbadis, Polyspike ictal onset absence seizures, *J. Clin. Neurophysiol.*, **27** (2010), 93–99. https://doi.org/10.1097/WNP.0b013e3181d64b1d
6. J. F. Barry, M. J. Turner, J. M. Schloss, D. R. Glenn, Y. Song, M. D. Lukin, et al., Optical magnetic detection of single-neuron action potentials using quantum defects in diamond, *Proc. Natl. Acad. Sci.*, **113** (2016), 14133–14138. https://doi.org/10.1073/pnas.1601513113
7. J. Ma, J. Tang, A review for dynamics in neuron and neuronal network, *Nonlinear Dyn.*, **89** (2017), 1569–1578. https://doi.org/10.1007/s11071-017-3565-3
8. M. Lv, J. Ma, Multiple modes of electrical activities in a new neuron model under electromagnetic radiation, *Neurocomputing*, **205** (2016), 375–381. https://doi.org/10.1016/j.neucom.2016.05.004
9. M. Lv, C. Wang, G. Ren, J. Ma, J. Song, Model of electrical activity in a neuron under magnetic flow effect, *Nonlinear Dyn.*, **85** (2016), 1479–1490. https://doi.org/10.1007/s11071-016-2773-6
10. M. Ge, L. Lu, Y. Xu, X. Zhan, L. Yang, Y. Jia, Effects of electromagnetic induction on signal propagation and synchronization in multilayer Hindmarsh-Rose neural networks, *Eur. Phys. J. Spec. Top.*, **228** (2019), 2455–2464. https://doi.org/10.1140/epjst/e2019-900049-0
11. N. Zandi-Mehran, S. Jafari, S. M. R. Hashemi Golpayegani, F. Nazarimehr, M. Perc, Different synaptic connections evoke different firing patterns in neurons subject to an electromagnetic field, *Nonlinear Dyn.*, **100** (2020), 1809–1824. https://doi.org/10.1007/s11071-020-05568-9
12. F. Wu, H. Gu, Y. Li, Inhibitory electromagnetic induction current induces enhancement instead of reduction of neural bursting activities, *Commun. Nonlinear Sci. Numer. Simul.*, **79** (2019), 104924. https://doi.org/10.1016/j.cnsns.2019.104924
13. F. Wu, J. Ma, G. Zhang, A new neuron model under electromagnetic field, *Appl. Math. Comput.*, **347** (2019), 590–599. https://doi.org/10.1016/j.amc.2018.11.035
14. L. Duan, Q. Cao, Z. Wang, J. Su, Dynamics of neurons in the pre-bötzinger complex under magnetic flow effect, *Nonlinear Dyn.*, **94** (2018), 1961–1971. https://doi.org/10.1007/s11071-018-4467-8

15. Z. X. Yuan, P. H. Feng, M. M. Du, Y. Wu, Dynamical response of a neuron-astrocyte coupling system under electromagnetic induction and external stimulation, *Chin. Phys. B*, **29** (2020), 030504. https://doi.org/10.1088/1674-1056/ab69d0
16. F. Zhang, A. M. Aravanis, A. Adamantidis, L. de Lecea, K. Deisseroth, Circuit-breakers: optical technologies for probing neural signals and systems, *Nat. Rev. Neurosci.*, **8** (2007), 577–581. https://doi.org/10.1038/nrn2192
17. Z. Shen, Z. Deng, L. Yan, Y. Zhao, L. Du, H. Zhang, Transition dynamics and optogenetic control of epileptiform activity in a modified mean filed model of human cortex, *Commun. Nonlinear Sci. Numer. Simul.*, **116** (2023), 106812. https://doi.org/10.1016/j.cnsns.2022.106812
18. K. Nikolic, P. Degenaar, C. Toumazou, Modeling and engineering aspects of channelrhodopsin2 system for neural photostimulation, in *2006 International Conference of the IEEE Engineering in Medicine and Biology Society*, (2006), 1626–1629. https://doi.org/10.1109/IEMBS.2006.259737
19. P. Selvaraj, J. W. Sleigh, W. J. Freeman, H. E. Kirsch, A. J. Szeri, Open loop optogenetic control of simulated cortical epileptiform activity, *J. Comput. Neurosci.*, **36** (2014), 515–525. https://doi.org/10.1007/s10827-013-0484-2
20. P. Selvaraj, J. W. Sleigh, H. E. Kirsch, A. J. Szeri, Closed-loop feedback control and bifurcation analysis of epileptiform activity via optogenetic stimulation in a mathematical model of human cortex, *Phys. Rev. E*, **93** (2016), 012416. https://doi.org/10.1103/PhysRevE.93.012416
21. X. Wang, Y. Yu, Q. Wang, Modeling the modulation of beta oscillations in the basal ganglia by dual-target optogenetic stimulation, *Fundam. Res.*, (2024). https://doi.org/10.1016/j.fmre.2024.01.015
22. P. N. Taylor, Y. Wang, M. Goodfellow, J. Dauwels, F. Moeller, U. Stephani, et al., A computational study of stimulus driven epileptic seizure abatement, *PLOS One*, **9** (2014), e114316. https://doi.org/10.1371/journal.pone.0114316
23. J. Zhao, Y. Yu, F. Han, Q. Wang, Regulating epileptiform discharges by heterogeneous interneurons in thalamocortical model, *Chaos*, **33** (2023), 083121. https://doi.org/10.1063/5.0156151
24. J. Paz, T. Davidson, E. Frechette, B. Delord, L. Parada, K. Peng, Closed-loop optogenetic control of thalamus as a tool for interrupting seizures after cortical injury, *Nat. Neurosci.*, **16** (2013), 64–70. https://doi.org/10.1038/nn.3269
25. E. Krook-Magnuson, C. Armstrong, M. Oijala, I. Soltesz, On-demand optogenetic control of spontaneous seizures in temporal lobe epilepsy, *Nat. Commun.*, **4** (2013), 1376. https://doi.org/10.1038/ncomms2376
26. K. Nikolic, N. Grossman, M. S. Grubb, J. Burrone, C. Toumazou, P. Degenaar, Photocycles of channelrhodopsin-2, *Photochem. Photobiol.*, **85** (2009), 400–411. https://doi.org/10.1111/j.1751-1097.2008.00460.x
27. J. C. Williams, J. Xu, Z. Lu, A. Klimas, X. Chen, C. M. Ambrosi, et al., Computational optogenetics: Empirically-derived voltage- and light-sensitive channelrhodopsin-2 model, *PLoS Comput. Biol.*, **9** (2013), e1003220. https://doi.org/10.1371/journal.pcbi.1003220
28. Y. Che, Distributed open-loop optogenetic control of cortical epileptiform activity in a Wilson-Cowan network, in *2017 8th International IEEE/EMBS Conference on Neural Engineering (NER)*, (2017), 469–472. https://doi.org/10.1109/NER.2017.8008389

29. H. Zhang, Z. Shen, Y. Zhao, L. Du, Z. Deng, Dynamical mechanism analysis of three neuroregulatory strategies on the modulation of seizures, *Int. J. Mol. Sci.*, **23** (2022), 13652. https://doi.org/10.3390/ijms232113652
30. D. Fan, F. Liao, Q. Wang, The pacemaker role of thalamic reticular nucleus in controlling spike-wave discharges and spindles, *Chaos*, **27** (2017), 073103. https://doi.org/10.1063/1.4991869
31. D. Fan, S. Liu, Q. Wang, Stimulus-induced epileptic spike-wave discharges in thalamocortical model with disinhibition, *Sci. Rep.*, **6** (2016), 37703. https://doi.org/10.1038/srep37703
32. Y. Ge, Y. Cao, G. Yi, C. Han, Y. Qin, J. Wang, et al., Robust closed-loop control of spike-and-wave discharges in a thalamocortical computational model of absence epilepsy, *Sci. Rep.*, **9** (2019), 9093. https://doi.org/10.1038/s41598-019-45647-5
33. S. Panthi, B. Leitch, Chemogenetic activation of feed-forward inhibitory parvalbumin-expressing interneurons in the cortico-thalamocortical network during absence seizures, *Front. Cell. Neurosci.*, **15** (2021), 688905. https://doi.org/10.3389/fncel.2021.688905
34. A. Brodovskaya, J. Kapur, Anticonvulsant dopamine type 2 receptor agonist activates inhibitory parvalbumin interneurons, *Epilepsia*, **62** (2021), e147–e152. https://doi.org/10.1111/epi.17024
35. X. Jiang, A. Lupien-Meilleur, S. Tazerart, M. Lachance, E. Samarova, R. Araya, et al., Remodeled cortical inhibition prevents motor seizures in generalized epilepsy, *Ann. Neurol.*, **84** (2018), 436–451. https://doi.org/10.1002/ana.25301
36. C. Tai, Y. Abe, R. E. Westenbroek, T. Scheuer, W. A. Catterall, Impaired excitability of somatostatin- and parvalbumin-expressing cortical interneurons in a mouse model of Dravet syndrome, *Proc. Natl. Acad. Sci. U.S.A.*, **111** (2014), E3139–E3148. https://doi.org/10.1073/pnas.1411131111
37. S. Liang, T. Zhang, S. Wu, Z. Chen, The dynamical role of electromagnetic induction in epileptic seizures: a double-edged sword, *Nonlinear Dyn.*, **106** (2021), 975–988. https://doi.org/10.1007/s11071-021-06911-4
38. E. Krook-Magnuson, I. Soltesz, Beyond the hammer and the scalpel: selective circuit control for the epilepsies, *Nat. Neurosci.*, **18** (2015), 331–338. https://doi.org/10.1038/nn.3943

AIMS Press